

**Real-space observation of current-driven domain wall motion in submicron
magnetic wires**

Akinobu Yamaguchi^{*1}, Teruo Ono¹, Saburo Nasu¹, Kousaku Miyake², Ko Mibu³, and
Teruya Shinjo⁴

¹ Graduate School of Engineering Science, Osaka University, Toyonaka 560-8531,
Japan

² Institute for Chemical Research, Kyoto University, Uji 611-0011, Japan

³Research Center for Low Temperature and Materials Sciences, Kyoto University, Uji
611-0011, Japan

⁴International Institute for Advanced Studies, Soraku-gun, 619-0225, Japan

^{*}e-mail:akinobu@moss.mp.es.osaka-u.ac.jp

Spintronic devices, whose operation is based on the motion of a magnetic domain wall (DW), have been proposed recently^{1, 2}. If a DW could be driven directly by flowing an electric current instead of a magnetic field, the performance and functions of such device would be drastically improved. Here we report real-space observation of the current-driven DW motion by using a well-defined single DW in a micro-fabricated magnetic wire with submicron width. Magnetic force microscopy (MFM) visualizes that a single DW introduced in the wire is displaced back and forth by positive and negative pulsed-current, respectively. We can control the DW position in the wire by tuning the intensity, the duration and the polarity of the pulsed-current. It is, thus, demonstrated that spintronic device operation by the current-driven DW motion is possible.

In general, ferromagnets are composed of magnetic domains, within each of which magnetic moments align. The directions of magnetization of neighboring domains are not parallel. As a result, there is a magnetic DW between neighboring domains. The direction of moments gradually changes in a DW. What will happen if an electric current flows through a DW? Since the spin direction of conduction electrons changes when the electrons cross the DW, spin transfer from electrons into the DW occurs and torque is exerted on the DW. In consequence, the electric current can displace the DW^{3, 4}. This current-driven DW motion has been confirmed by experiments on magnetic thin films and patterned films with multi-domain structures⁵⁻⁸. The current-driven DW motion in a magnetic wire with submicron width, which is of importance for practical applications, has been reported very recently^{9, 10}. However, quantitative experiments on a single DW in a magnetic wire are needed to get deeper insights into the physical mechanisms of this effect, which leads to an efficient operation of DW devices. Our real-space observation by MFM gives the quantitative information: DW displacement as a function of the intensity and the duration of the pulsed-current.

We designed a special L-shaped magnetic wire with a round corner as schematically illustrated in Fig. 1. One end of the L-shaped magnetic wire is connected to a diamond-shaped pad which acts as a DW injector¹¹, and the other end is sharply pointed to prevent a nucleation of a DW from this end¹². L-shaped magnetic wires of 10 nm-thick Ni₈₁Fe₁₉ were fabricated onto thermally oxidized Si substrates by means of an e-beam lithography and a lift-off method. The width of the wire is 240 nm. The wire has four electrodes made of nonmagnetic material, 20 nm-thick Cu, for electrical transport measurements. MFM observations were performed for the hatched area in Fig. 1 at room temperature. CoPtCr low moment probes were used in order to minimize the influence of the stray field from the probe on the DW in the wire.

Because of the special shape of the wire, a single DW can be introduced from the diamond-shaped pad and it stops in the vicinity of the round corner when a magnetic field is applied along the wire axis connected to the pad^{11, 13}. In order to introduce a DW at the position a little bit away from the corner, the direction of the external magnetic field was set 26 degrees from the wire axis in the substrate plane as shown in Fig.1. In the initial stage, a magnetic field of +1 kOe was applied in order to align the magnetization in one direction along the wire. Then, a single DW was introduced by applying a magnetic field of -175 Oe. After that, the MFM observations were carried out in the absence of a magnetic field. The existence of the single DW in the vicinity of the corner was confirmed as shown in Fig. 2a. The DW is imaged as a bright contrast, which corresponds to the stray field from positive magnetic charge. In this case, a head-to-head DW is realized as schematically illustrated in Fig. 2b. The position and the shape of the DW were unchanged after several MFM scans, indicating that the DW was pinned by a local structural defect and that a stray field from the probe was too small to change the magnetic structure and position of the DW.

To clarify the magnetic structure of the head-to-head DW, micromagnetics simulations were performed by using micromagnetics simulator (OOMMF) from NIST¹⁴. The parameters used for the calculation were a unit cell size of 5 nm × 5 nm with a constant thickness of 10 nm, a magnetization of 1.08 T, and a damping constant of $\alpha = 0.1$. The size of the calculated model was the same as the sample for the experiment except for the length of the wire. Two types of DWs, vortex and transverse DW, were obtained as a stable state in the absence of a magnetic field by changing the initial magnetization configuration. Figures 2c and 2d show the results of the micromagnetics simulations for the vortex and the transverse DW, respectively. Figures 2e and 2f show the MFM images calculated from the magnetic structures¹⁵ shown in Figs. 2c and 2d, respectively. By comparing the calculated MFM images with the observed

high-resolution MFM image of the DW (Fig. 2g), it is concluded that the DW is the vortex type.

After the observation of Fig. 2a, a pulsed-current was applied through the wire in the absence of a magnetic field. The current density and the pulse duration were $1.2 \times 10^{+12} \text{ A/m}^2$ and $5 \mu\text{s}$, respectively, and the rise and fall times were shorter than 15 ns. Figure 2h shows the MFM image after an application of the pulsed-current from left to right. The DW, which had been in the vicinity of the corner (Fig. 2a), was displaced from right to left by the application of the pulsed-current. Thus, the direction of the DW motion is opposite to the current direction. Furthermore, the direction of the DW motion can be reversed by switching the current polarity as shown in Fig. 2i. These results are consistent with the spin transfer mechanism^{3,4}.

Figures 3a-3k are successive MFM images with one pulsed-current applied between each consecutive image. The current density and the pulse duration were $1.2 \times 10^{+12} \text{ A/m}^2$ and $0.5 \mu\text{s}$, respectively. Prior to the MFM observation, a magnetic field of -1 kOe was applied in order to align the magnetization in the direction opposite to that in the previous experiment. Then, a tail-to-tail DW was introduced by applying a magnetic field of +175 Oe. The introduced DW is imaged as a dark contrast in Fig. 3, which indicates that a tail-to-tail DW is formed as schematically illustrated in Fig. 3. The direction of the tail-to-tail DW motion is also opposite to the current direction. The fact that both head-to-head and tail-to-tail DWs are displaced opposite to the current direction clearly indicates that the DW motion is not caused by a magnetic field generated by the current (Oersted field). Each pulse displaced the DW opposite to the current direction. The difference in the displacement for each pulse is possibly due to the pinning by randomly located defects. The average displacement per one pulse did not depend on the polarity of the pulsed-current.

We discuss the interpretation of the observed current-driven DW motion. First, we can rule out the effect of the Joule heating by the pulsed-current, since the heating

cannot explain the fact that the direction of the DW motion is reversed by switching the current polarity. The effect of the Oersted field is also ruled out as mentioned above. Hydromagnetic DW-drag force associated with the Hall effect is negligible in films thinner than $0.1 \mu\text{m}$ ¹⁶. Therefore, only the spin transfer mechanism^{3, 4} can explain our experimental results. The critical current density j_c below which the DW cannot be driven by the current was observed to be about $1.0 \times 10^{+12} \text{ A/m}^2$. MFM measurements under an external magnetic field revealed that the critical magnetic field H_c of about 30 Oe was needed to move the DW. Thus, a force per unit current of $5.1 \times 10^{-10} \text{ N/A}$ is obtained by using the expression $2M_sH_c/j_c$, where M_s is the saturation magnetization of $\text{Ni}_{81}\text{Fe}_{19}$ ⁶. This is comparable to the reported values^{6, 10}.

For more quantitative discussion, we investigated the DW displacement as a function of the duration and the intensity of the pulsed-current. Figure 4a shows the average DW displacement per one pulse as a function of the pulse duration under a condition of constant current density of $1.2 \times 10^{+12} \text{ A/m}^2$. The average DW displacement is proportional to the pulse duration, which indicates that the DW has a constant velocity of 3.0 m/s and the motion of the DW is in viscous regime. Figure 4b shows the average DW velocity as a function of the current density. The average velocity could be determined only in a narrow range of the current density from $1.1 \times 10^{+12} \text{ A/m}^2$ to $1.3 \times 10^{+12} \text{ A/m}^2$. Below $1.1 \times 10^{+12} \text{ A/m}^2$, the displacement for each pulse was not reproducible. Above $1.3 \times 10^{+12} \text{ A/m}^2$, the samples were degraded by the Joule heating due to the high current density. Although the DW velocity was measured only in the small current density range, it was well confirmed that the DW velocity increases with the current density, as expected from the spin transfer mechanism.

We discuss the efficiency of the current-driven DW motion in the present experiments. Since the DW width in the present experiment is much larger than the Larmor precession length (several nm), the electron's spin can adiabatically follow the direction of the local magnetization⁴. As a result, each electron passing through the DW

flips its spin and gives a quantum h of angular momentum to the DW. This spin transfer adds magnetic moment of $2\mu_B$ to the DW, where μ_B is the Bohr magneton. Thus, the expected change of magnetic moment in the wire by the pulsed-current, m_{current} , is calculated as $m_{\text{current}} = 2p\mu_B j S \Delta t / e$, where p is the spin-polarization of the current, j is the current density, S is the cross-sectional area of the wire, Δt is the pulse duration, and e is the electronic charge. On the other hand, the change of magnetic moment in the wire by the displacement of the DW, Δm , is calculated as $\Delta m = M_s \Delta l S$, where Δl is the displacement of the DW. Thus, we define the efficiency as $\eta = \Delta m / m_{\text{current}}$. From the definition, the efficiency is zero below j_c because the DW does not move below j_c . This means the transferred spin angular momentum dissipates into the environment possibly through the excitation of local spin waves in the DW. The efficiency increases with the current density and $\eta = 0.05$ at $j = 1.3 \times 10^{12} \text{ A/m}^2$ if we assume $p = 0.7^{17}$. Apparently, the higher efficiency will be achieved by decreasing H_c because j_c is reduced.

We have shown the current-driven DW motion for a single DW with a well-defined magnetic structure in a submicron magnetic wire, which certifies the spintronic device operation by this effect. All experimental results are consistent with the spin transfer mechanism^{3, 4}. We hope our quantitative findings stimulate the theoretical works on the current-driven DW motion. Micromagnetics simulation which incorporates the spin transfer mechanism is useful to understand the present result, because the direct MFM observation clarified not only the DW displacement as a function of the intensity and the duration of the pulsed-current but also the internal structure of the DW.

References

1. Versluijs, J. J. *et al.* Magnetoresistance of Half-Metal Oxide Nanocontact. *Phys. Rev. Lett.* **87**, 0266011-0266014 (2001).
2. Allwood, D. A. *et al.* Submicrometer Ferromagnetic NOT Gate and Shift Register. *Science* **296**, 2003-2006 (2002).
3. Berger, L. Exchange interaction between ferromagnetic domain wall and electric current in very thin metallic films. *J. Appl. Phys.* **55**, 1954-1956 (1984).
4. Waintal, X. & Viret, M. Current induced distortion of a magnetic domain wall. *cond-mat/031293* (2003).
5. Freitas, P. P. & Berger, L. Observation of s-d exchange force between domain walls and electric current in very thin Permalloy films. *J. Appl. Phys.* **57**, 1266-1269 (1985).
6. Hung, C. -Y. & Berger, L. Exchange forces between domain wall and electric current in permalloy films of variable thickness. *J. Appl. Phys.* **63**, 4276-4278 (1988).
7. Gan, L. *et al.* Pulsed-Current-Induced Domain Wall Propagation in Permalloy Patterns Observed Using Magnetic Force Microscope. *IEEE Tran. Magn.* **36**, 3047-3049 (2000).
8. Koo, H. *et al.* Current controlled bi-stable domain configuration in Ni₈₁Fe₁₉ elements: An approach to magnetic memory devices. *Appl. Phys. Lett.* **81**, 862-864 (2002).
9. Grollier, J. *et al.* Switching a spin-valve back and forth by current-induced domain wall motion. *cond-mat/0304312* (2003).

10. Vernier, N. *et al.* Domain wall propagation in magnetic nanowires by spin polarized current injection. *cond-mat/0304549* (2003).
11. Shigeto, K *et al.* Injection of a magnetic domain wall into a submicron magnetic wire. *Appl. Phys. Lett.* **75**, 2815-2817 (1999).
12. Schrefl, T *et al.* Domain structures and switching mechanisms in patterned magnetic elements. *J. Magn. Magn. Mater.* **175**, 193-204 (1997).
13. Allwood, D. A. *et al.* Shifted hysteresis loops from magnetic nanowires. *Appl. Phys. Lett.* **81**, 4005-4007 (2002).
14. <http://math.nist.gov/oommf/>.
15. Saito, H *et al.* Description of magnetic force microscopy by three-dimensional tip Green's function for sample magnetic charges. *J. Magn. Magn. Mater.* **191**, 153-161 (1999).
16. Berger, L. LOW-FIELD MAGNETORESISTANCE AND DOMAIN DRAG IN FERROMAGNETS. *J. Appl. Phys.* **49**, 2156-2161 (1978).
17. Bass, J. & Pratt, W.P. Jr. Current-perpendicular (CPP) magnetoresistance in magnetic metallic multilayers. *J. Magn. Magn. Mater.* **200**, 274-289 (1999).

Acknowledgements

We would like to thank Y. Suzuki, S. Yuasa, H. Kohno, and G. Tatara for valuable discussions. The present work was partly supported by the Ministry of Education, Culture, Sports, Science and Technology of Japan (MEXT), through the Grants-in-Aid for COE Research (10CE2004 and 12CE2005) and MEXT Special Coordination Funds

for Promoting Science and Technology (Nanospintronics Design and Realization, NDR).

Correspondence and requests for materials should be addressed to A.Y. (e-mail: akinobu@moss.mp.es.osaka-u.ac.jp).

Competing financial interests

The authors declare that they have no competing financial interests.

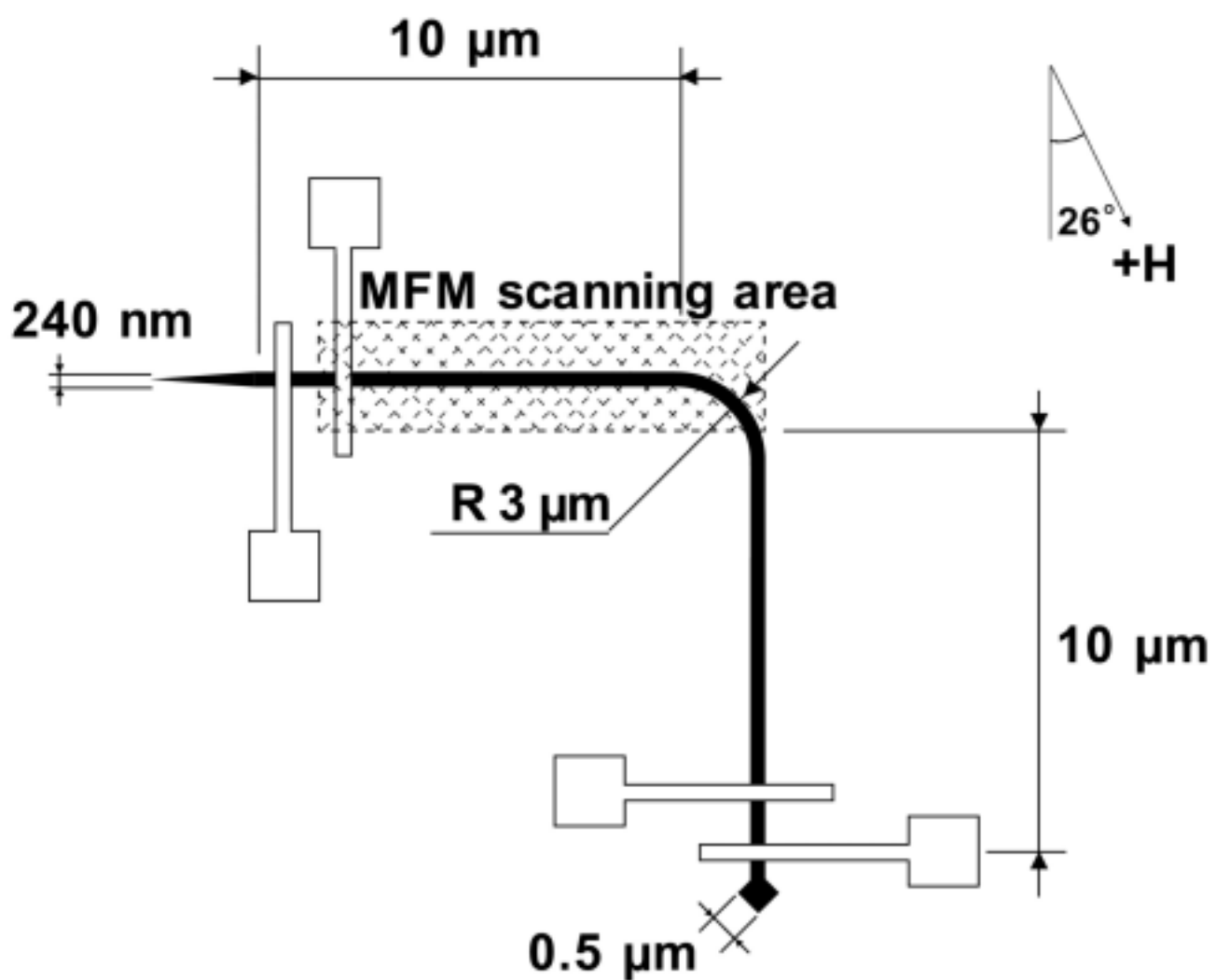
Figure captions

Figure 1 : Schematic illustration of a top view of the sample. One end of the L-shaped wire is connected to a diamond-shaped pad which acts as a domain wall (DW) injector, and the other end is sharply pointed to prevent a nucleation of a DW from this end. The wire has four electrodes made of Cu. MFM observations were performed for the hatched area at room temperature.

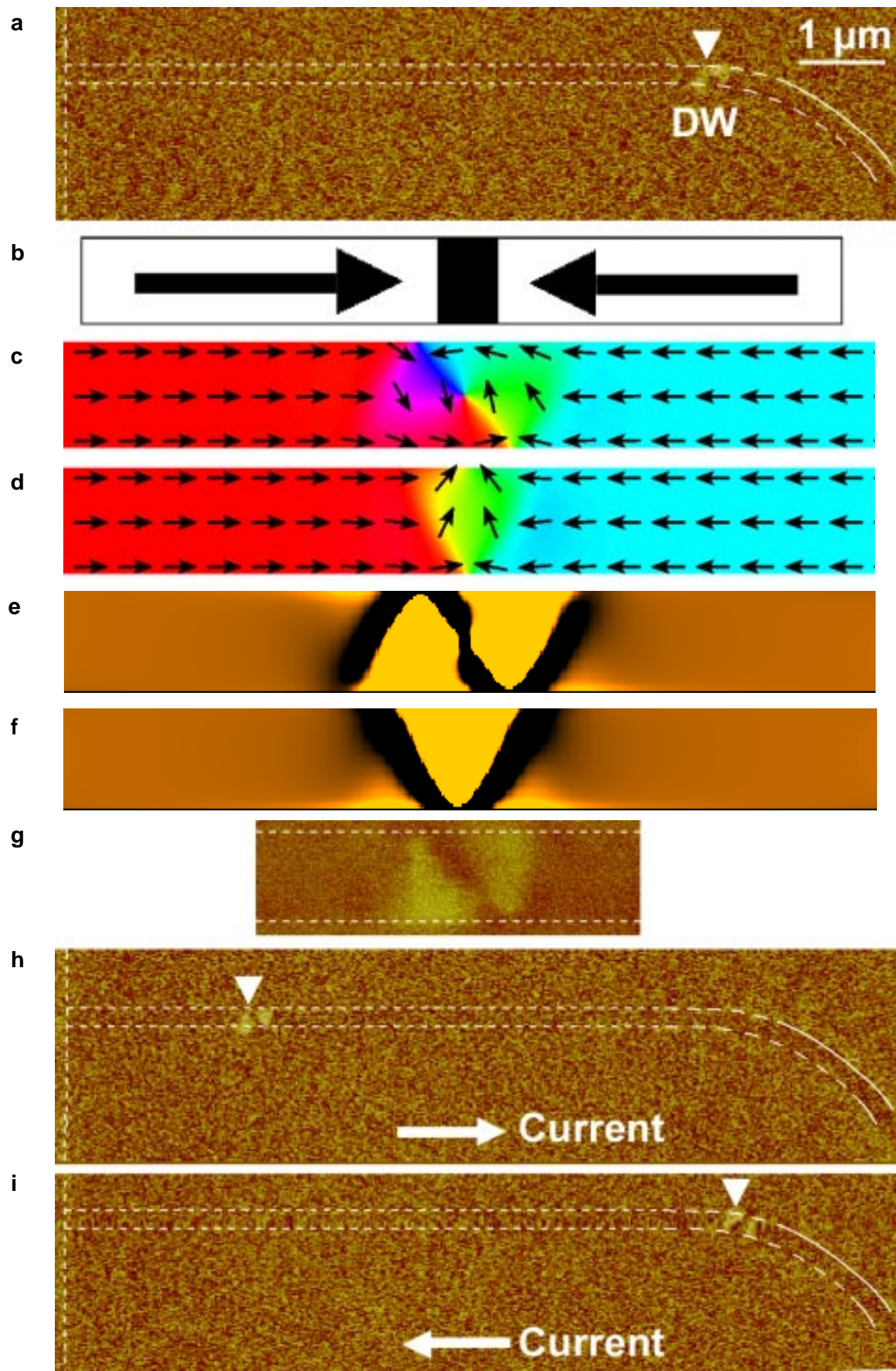
Figure 2 (color) : **a**, MFM image after the introduction of a DW. DW is imaged as a bright contrast, which corresponds to the stray field from positive magnetic charge. **b**, Schematic illustration of a magnetic domain structure inferred from the MFM image. DW has a head-to-head structure. **c**, Result of micromagnetics simulation (vortex DW). **d**, Result of micromagnetics simulation (transverse DW). **e**, MFM image calculated from the magnetic structure shown in Fig. 2c. **f**, MFM image calculated from the magnetic structure shown in Fig. 2d. **g**, Magnified MFM image of a DW. **h**, MFM image after an application of a pulsed-current from left to right. The current density and pulse duration are $1.2 \times 10^{+12} \text{ A/m}^2$ and 5 μs , respectively. DW is displaced from right to left by the pulsed-current. **i**, MFM image after an application of a pulsed-current from right to left. The current density and pulse duration are $1.2 \times 10^{+12} \text{ A/m}^2$ and 5 μs , respectively. DW is displaced from left to right by the pulsed-current.

Figure 3 (color) : **a-k**, Successive MFM images with one pulse applied between each consecutive image. The current density and the pulse duration were $1.2 \times 10^{+12} \text{ A/m}^2$ and $0.5 \mu\text{s}$, respectively. Note that a tail-to-tail DW is introduced, which is imaged as a dark contrast.

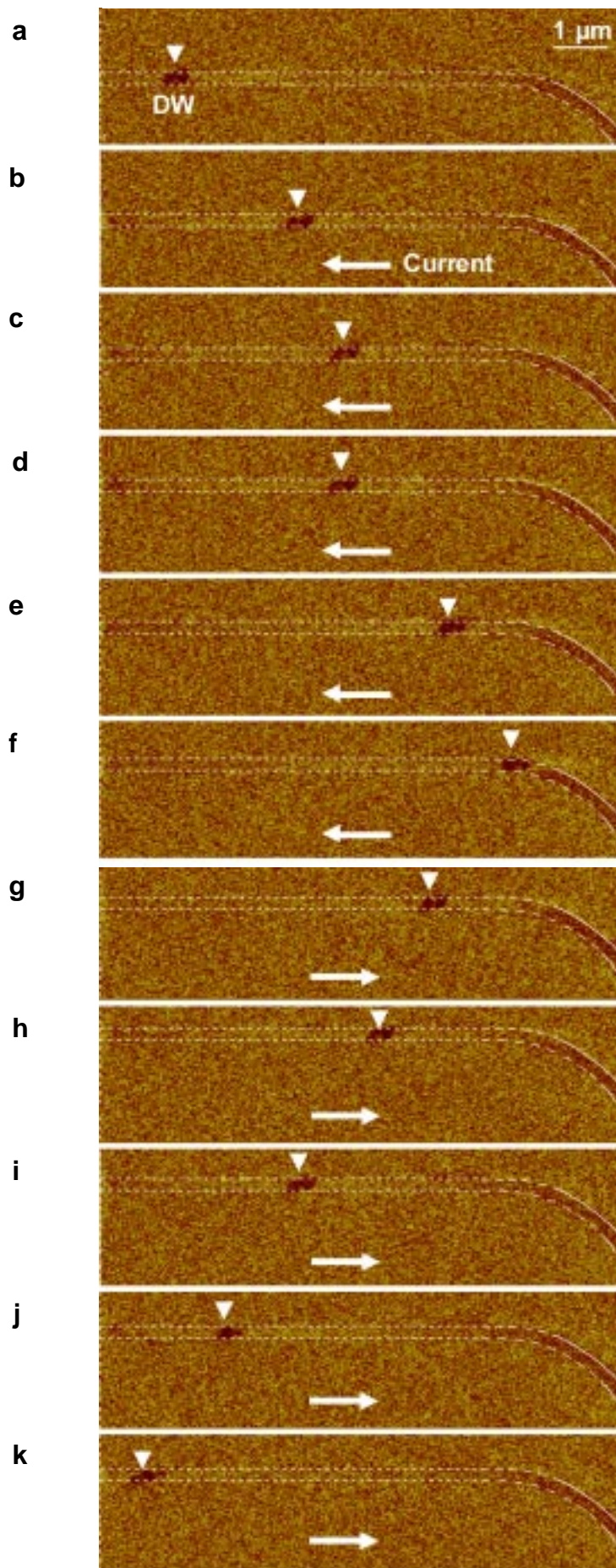
Figure 4 (color) : **a**, Average DW displacement per one pulse as a function of the pulse duration under a condition of constant current density of $1.2 \times 10^{+12} \text{ A/m}^2$. **b**, Average DW velocity as a function of the current density.



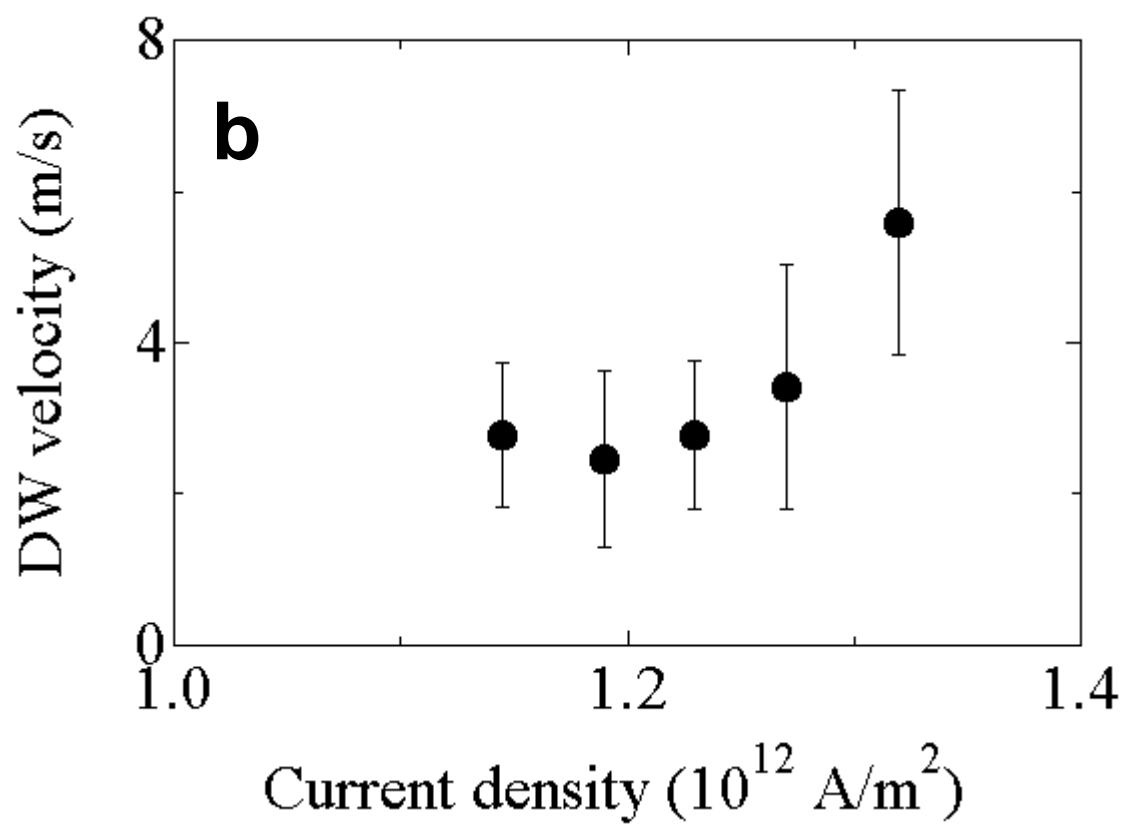
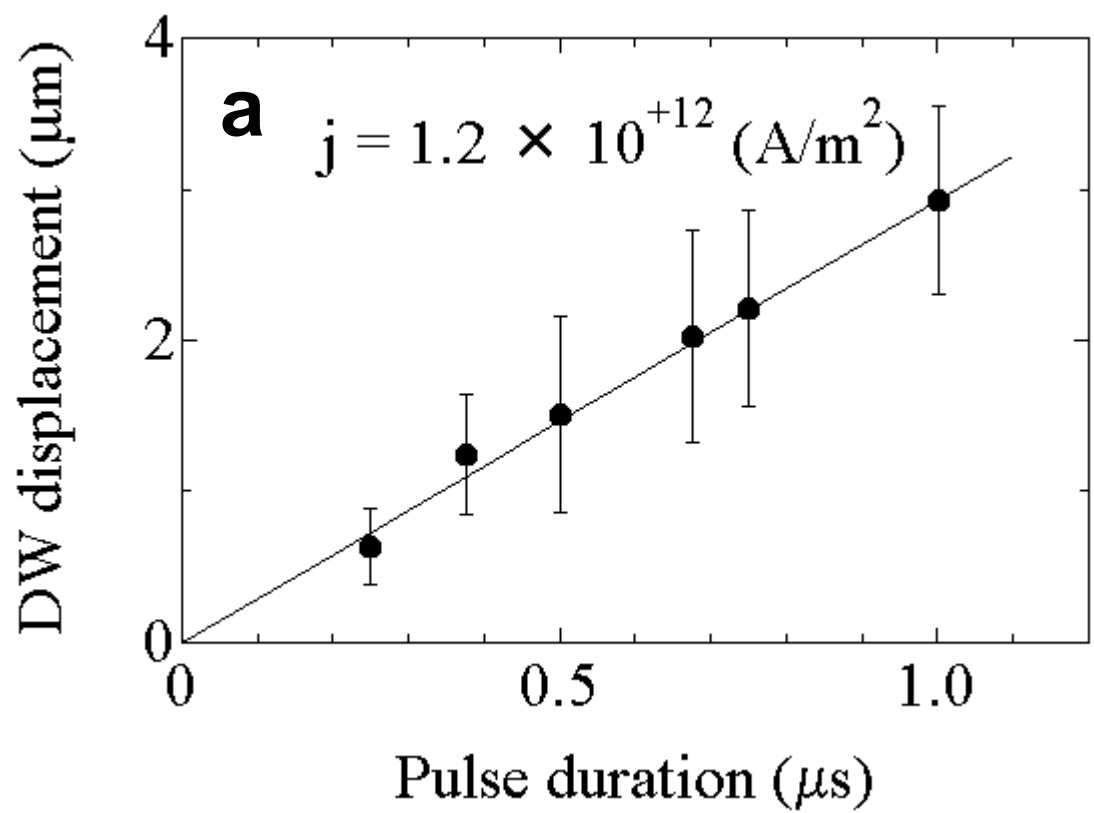
yamaguchi_Fig. 1



yamaguchi_Fig.2



yamaguchi_Fig.3



yamaguchi_Fig.4